Large Eddy Simulation of a single-injector LOx/GCH_4 combustion chamber using Analytically Reduced Chemistry

By S. Blanchard† & B. Cuenot

CERFACS - 42 Avenue Gaspard Coriolis, 31057 Toulouse, France

The LOx/GCH_4 single-injector combustion chamber developed at the Technical University Munich is simulated by using Large-Eddy Simulation (LES). The main objective is to study the impact of methane oxycombustion chemical kinetics in a typical rocket engine: high pressure, high strain rate flow. To do so, an Analytically Reduced Chemistry (ARC) is specifically derived for this test case. The ARC is validated by comparison with its parent skeletal mechanism on a series of laminar flames at conditions representative of the target LES configuration. To address the issue of numerical stiffness of oxycombustion, an original approach for time integration of chemistry is proposed, allowing to run the simulation at the CFL timestep. It is demonstrated on 1D and 2D laminar cases that the flame structure is well preserved, and that stability is ensured by decreasing CPU cost at the same time. Finally, the ARC for methane oxycombustion is combined with the proposed time integration method to compute the experimental combustion chamber. Results show a purely non-premixed turbulent flame, with a complex chemical structure. It is found that the proposed time integration method for chemistry allows a substantial gain of computational cost.

1. Introduction

The space launchers market knows right now a noticeable evolution. New private actors have started a price race in order to decrease the space access cost. The historical actors, mainly governmental space agencies, are therefore challenged to propose cheaper but still reliable solutions for commercial launches. To reach such objective the usual technical approaches must be questioned. This is the case for propulsion systems, which are even more challenged by the concept of reusability [1]. One solution largely considered in the community is to use methane instead of hydrogen in Liquid Rocket Engines (LRE). The reason is that methane brings some advantages such as high density, good specific impulse and lower cost for production and storage, which largely compensate a lower energy per unit mass compared to hydrogen [2–4]. Many projects of methane/oxygen-fed LRE for commercial launches as well as deep space missions, have appeared throughout the world, e.g. Prometheus (CNES/ArianeGroup), Raptor (SpaceX), or the LNG family (Jaxa/IHI) [5]. However, except for some early research in the 1970s-1990s [6], most studies of methane oxycombustion in rocket engines conditions are quite recent and many questions remain unsolved [7].

† also at Centre National d'Etudes Spatiales / Direction des Lanceurs - 52 rue Jacques Hillairet, 75612 Paris, France

In this context the Technical University of Munich has developed several methane-fed sub-scale rocket combustor test benches. Until recently, only GOx/GCH4 hot firing tests were performed with different configurations (single-, five- and seven-injectors in square or circular sections [8, 9]). In order to come closer to the real rocket engine conditions, a modification of the gaseous single-injector test bench has been made to allow LOx/GCH4 hot firing tests [10]. The objective is to provide experimental data to the scientific community, for better understanding and for assessment of models and numerical codes.

Large Eddy Simulation (LES) has been successfully applied to LRE to predict the flame, its ignition, wall heat transfer or thermo-acoustic instabilities [11–13]. Most studies were however considering hydrogen oxycombustion, which is close to the infinitely fast chemistry limit and may be largely simplified. The situation is different with methane oxycombustion, whose slower chemistry may impact combustion phenomena [14]. It is therefore necessary to include an accurate, but still cost-effective description of the combustion kinetics. There exists a wide range of kinetic schemes, from fully detailed mechanisms, containing hundreds to thousands species and reactions, to the most simple ones which only contain few species and two to four reactions. As any chemical species requires to solve one additional transport equation in the CFD code, the direct integration of detailed mechanisms is computationally unaffordable in 3D simulations. Even the so-called skeletal mechanisms which are much reduced compared to detailed ones, are still too CPU demanding. On the contrary, one- or two-steps kinetic schemes are really cheap but cruelly lack of precision.
As an alternative, the chemical kinetics community introduced some decades ago the concept of Analytically Reduced Chemistry (ARC) [15]. An ARC scheme derives from a skeletal mechanism, in which only the most relevant species and reactions are kept for a considered target: integral of heat release, adiabatic flame temperature, or flame speed as examples. ARC then introduces the Quasi Steady State Assumption (QSSA) [16] for the species that are immediately consumed after production, and introduce strong numerical stiffness due to their very short timescale. These QSSA species are kept but not computed with a transport equation : their concentration is calculated from algebraic relations issuing from their zero net chemical source term. The ARC approach has already shown promising results on diverse applications [17, 18].
Some ARC schemes already exist in the literature for methane combustion [19] but they have been mostly derived for combustion of CH_4 with air. In addition, an ARC scheme for oxycombustion in LRE must be valid at very high pressure and for highly strained non-premixed flames. Therefore, a new ARC scheme must be derived for the target application of the present study, and this is the objective of the first part of this paper.
Another difficulty raised by methane oxycombustion in LES of LRE is the extremely small time scale of the flame due to the extreme conditions. Unfortunately, QSSA only avoids the stiffness of the fastest radicals, but does not help for the main oxydation paths which introduce timescales typically 10 times smaller than the flow time scale. Implicit integration is a standard way to tackle the problem but remains computationally expensive and raise the complexity of the code [20]. Thus, a second objective of this work is to propose an original time-integration method for the chemical source terms.

This paper is organized as follows. In Section 2, the derivation of an ARC mechanism for methane oxycombustion is derived for the TUM's LOx/GCH$_4$ test bench conditions. Then in Section 3, a new integration method for the chemical source term is proposed. Validations are made on 2D flames in AVBP and compared to CANTERA. The developments made are finally used on the test bench, Section 4. Conclusions and perspectives are finally given in Section 5.

2. Derivation of ARC for methane oxycombustion

2.1. *Methodology*

As introduced above the first objective is to derive an ARC that will be used specifically for the simulation of the TUM's LOx/GCH$_4$ test bench. The first step is to define a reference mechanism. The literature proposes a number of schemes, among which three have been tested: the GRI3.0 [21], the Ramec [22] and the Slavinskaya [23]. It was found that for the targeted operating condition ($P = 20bar$, high strain rate - see below), all schemes give similar results but the Ramec mechanism (38 species, 190 reactions) exhibits overall the larger chemical timestep and is therefore chosen as reference scheme for CPU time considerations. Furthermore, it was specifically made for the methane oxycombustion at high pressures.
Using diffusion flames as target flames for the reduction, the range of strain rate (or equivalently scalar dissipation rate, recalled Eq. 2.1) must be defined. It was here determined from a prior computation in a representative area, downstream of the lip of the injector as shown in Fig. 6, Section 4. To get an ARC which is robust to strain rate, highest values found around stoichiometry $0.195 < Z < 0.205$ are chosen (the mixture fraction at the stoichiometry is $Z_{st} = 0.2$ for methane oxycombustion), close to $\chi_{st} = 10000s^{-1}$.

$$\chi_{st} = 2D \left(\frac{\partial Z}{\partial x} \right)^2 \tag{2.1}$$

In addition, in order to be representative of the target configuration, the chemistry reduction is performed at $P = 20bar$, $T_{inlets} = 300K$ and a mixture ratio of 3 (detailed operating conditions are specified Table 4). These fixed parameters are quite restrictive and specific to the considered target application, but they allow a strong reduction of the number of species and reactions. Larger ranges of mixture ratio, scalar dissipation rate, pressure or temperature lead to a more flexible ARC valid in extended ranges of conditions, but reaching typically about 30 species for 130 reactions it does not represent a huge reduction.
The reduction algorithm ARCANE [24] (written in Python) is used with as main target the integral of heat release. This quantity is essential for diffusion flames as, similarly to the flame speed for premixed flames, it ensures a correct consumption speed, thus a correct flame length. The reduction is performed with a maximum error of 5% on the integral of heat release between the reference and the reduced scheme.

The reduction process goes through several steps. First, Direct Relation Graph with Error Propagation (DRGEP) is performed several times on the skeletal mechanism to keep only the most relevant species and reactions. Chemical lumping is then applied to remove the isomeric molecules. Finally a Level Of Importance (LOI) criterion is applied

on the remaining species to select the ones treated with the QSS assumption.
After the reduction process, a 20 transported species (19 reactive + N_2), 5 QSS and 69 reactions mechanism is obtained. The new reduced mechanism, detailed in Table 1, is now tested in CANTERA against the reference scheme to verify its good behaviour on the targeted operating point.

Transported	QSS
H2 H O O2 OH H2O HO2 H2O2 CH3 CH4 CO CO2 HCO CH2O CH3OH C2H2 C2H4 C2H5 C2H6 N2	CH2 CH3O C2H3 CH3O2 C2H5O2

TABLE 1. Species contained in the derived ARC

2.2. *Validation*

For all the following the mixture fraction Z is computed with Bilger's definition [25]. The profiles shown Fig. 1 show an excellent agreement between the Ramec and the ARC. The maximum temperature exhibits only 0.58% error; the maximum heat release 0.34%; and the integral of heat release 0.47%. Even not all shown here, the species profiles show as well an overall good agreement. The ARC also has good performances for premixed flames (<4% error for burnt gases temperature, heat release and flame speed) and 0D reactors.

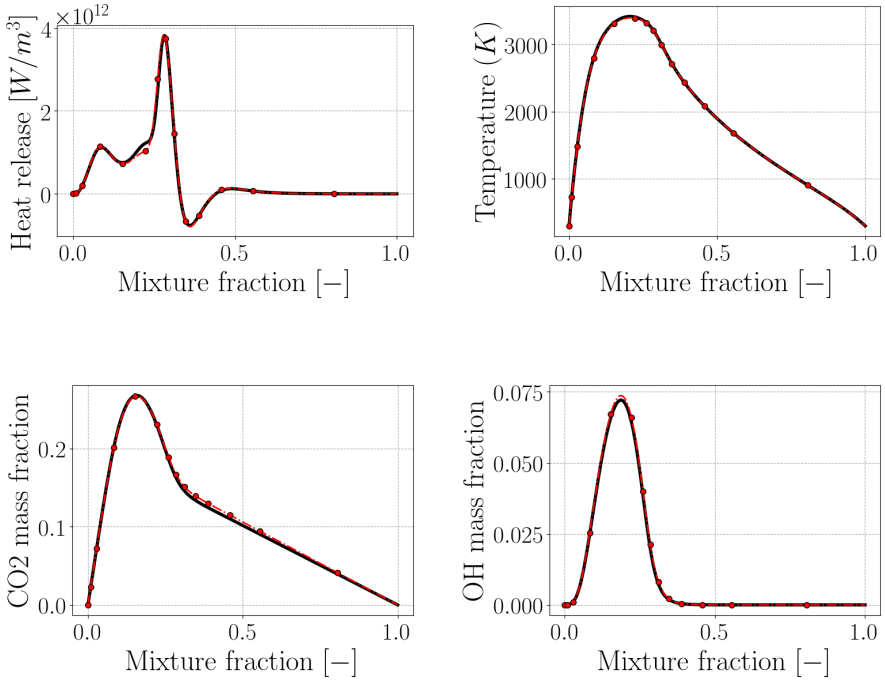

FIGURE 1. Comparison between the Ramec mechanism (thick line) and the derivated ARC (dashed-dotted line with round markers).

3. Time integration of chemistry

Although the strongest stiffness has been removed thanks to the QSSA applied to the fastest radicals, very small chemical time scales remain as methane oxycombustion at high pressure is a very fast oxydation process. Explicit time integration then requires a time step at least of the order of the shortest chemical timestep τ_{chem}, which may considerably increase the computing time. Flow simulations are run at the CFL timestep, and the objective is to keep this timestep for reacting flow simulations.
To do so a new time integration method for the chemical source term is proposed. The idea is to take advantage of the simple form of elementary reactions composing the ARC scheme to derive an analytical solution that is then introduced in the species transport equation.

We consider a specie k which is produced and consumed only by first order chemical reactions. By definition its net rate of variation $\dot{\omega}_k$ writes:

$$\dot{\omega}_k = A_k c_k + B_k, \tag{3.1}$$

with c_k the concentration of the species k, A_k its destruction term divided by c_k and B_k its creation term. The functions $A_k c_k$ and B_k are the sum of the contributions to destruction and creation respectively, of a reaction j involving the species k:

$$A_k c_k = \sum_{j=1}^{M} \dot{\omega}_{kj} \text{ for all } \dot{\omega}_{kj} < 0 \text{ and } B_k = \sum_{j=1}^{M} \dot{\omega}_{kj} \text{ for all } \dot{\omega}_{kj} > 0, \tag{3.2}$$

$\dot{\omega}_{kj}$ being the reaction rate of reaction j linked to the species k.
In a homogeneous reactor, c_k obeys the following evolution equation:

$$\frac{dc_k}{dt} = \dot{\omega}_k = A_k c_k + B_k \tag{3.3}$$

Assuming constant A_k and B_k, the solution to the above equation is easily found to be:

$$c_k = \left(c_{k,0} + \frac{B_k}{A_k} \right) e^{A_k t} - \frac{B_k}{A_k} \tag{3.4}$$

The above expression may be used to evaluate the solution at time iteration $n+1$ from the solution at time iteration n:

$$c_k^{n+1} = \left(c_k^n + \frac{B_k}{A_k} \right) e^{A_k \Delta t} - \frac{B_k}{A_k} \tag{3.5}$$

where Δt is the timestep of the simulation. If Δt is small enough, A_k and B_k may indeed be assumed constant during the time step and the above expression is a good guess of the solution at the next time iteration. It can be then introduced in the species transort equation by simply writing the source term as:

$$\dot{\omega}_k = \frac{c_k^{n+1} - c_k^n}{\Delta t} \tag{3.6}$$

Note that the expression for c_k in Eq. 3.4 is always positive (provided $c_{k,0}$ is positive), so that the approach guarantees positivity of all concentrations. Notice also that this expression only holds for first order reactions. For higher orders, the integration of the differential equation is still possible but the analytical solution becomes complex. As very

few reactions are not first order (8 over 69 in the previously derived ARC), the impact of using first order solution for them is considered negligible and Eq. 3.4 is kept for all reactions.
In the following, this method is named as "exponential" chemistry, which is now tested against direct explicit standard integration of the Arrhenius form, which will be called hereafter "classical" chemistry.

3.1. *Validation in a counterflow strained diffusion flame*

The obtained ARC combined with the new time integration method is first applied to a laminar diffusion flame for validation. The code AVBP is now used (described in Section 4.2.2) for the 2D counterflow diffusion flames presented Fig. 2. The mass flow rates are set so that the momentum is the same for both sides in order to get the stagnation plane at the center of the geometry where the mesh is the most refined. This is made in a very small domain ($H = 0.5mm$) to get a high strain rate while keeping the flow laminars. With this setup, the targeted mean strain rate is about:

$$a_{mean} = \frac{u_f + u_o}{H} = 4546s^{-1}. \tag{3.7}$$

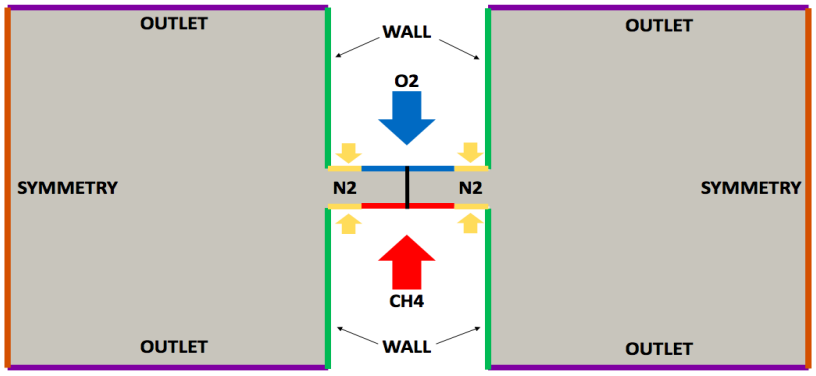

FIGURE 2. AVBP counterflow diffusion flame setup. The central thick vertical line indicates where the profiles are taken.

Because of numerical difficulties at the corners, a nitrogen coflow is used to help stabilizing the flame. Furthermore extra viscosity is added to avoid any perturbation which could destabilize the flow which is here laminar. This setup is computed twice: using the classical or the exponential integrations. Conditions are summarized in Table 2.

A fine mesh (about $\Delta = 1\mu m$ cell characteristic size at the stagnation plane) is first used to assess the exponential chemistry. Then a lower spatial resolution, about 10 times coarser which is more realistic of LES, allows to check if the exponential chemistry has the capacity to increase the computation timestep.
To compare the results of AVBP to CANTERA, a 1D CANTERA flame is computed with the prescribed value $a_{mean} = 4546s^{-1}$. Profiles from AVBP solution are taken along the central line of the setup shown in Fig. 2.

Pressure	[bar]	20
GOx mass flow rate	[g/s]	23.0
GCH4 mass flow rate	[g/s]	23.0
GN2 mass flow rate (per inlet)	[g/s]	2.3
GOx temperature	[K]	300
GCH4 temperature	[K]	300
GN2 temperature	[K]	300

TABLE 2. Operating point for the counterflow diffusion flame

3.1.1. *Fine mesh*

Results on the fine mesh are shown in Fig. 3.

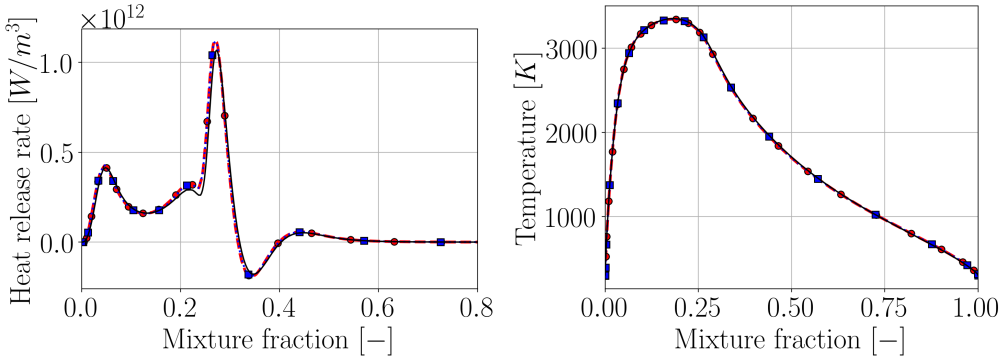

FIGURE 3. Heat release (left) and temperature (right) profiles in strained counterflow diffusion flame. Comparison between the classical (dashed-line), exponential (dotted-line) chemical integration methods and the CANTERA 1D flame (solid line). Fine mesh.

An excellent agreement between the classical, the exponential integration methods and the CANTERA 1D flame is found: actually exactly the same flame structure is retrieved. The deviation of the integral of heat release is only of 0.07% for the two AVBP computations; and a 4.5% difference between AVBP and CANTERA is found, which can be attributed to different numerical solvers and mesh resolution. In general, the global flame structure matches very well between classical and exponential chemistry and with theory.

3.1.2. *Coarse mesh*

Results on the coarse mesh are shown in Fig. 4.

Again the two integration methods are a good agreement. The heat release profiles are slighly different for example at $Z = 0.2$ and $Z = 0.35$ and the main peak does not reach the same maximum. However the integral of heat release is very close with a minor deviation of 0.71%. Note that the integral of heat release is about 50% higher than with the fine mesh: this is due to a higher scalar dissipation rate resulting from the artificial diffusion induced by the coarse mesh [26].

The use of a coarse mesh allows to increase the computation timestep and therefore test the exponential integration robustness. The simulation with the exponential chem-

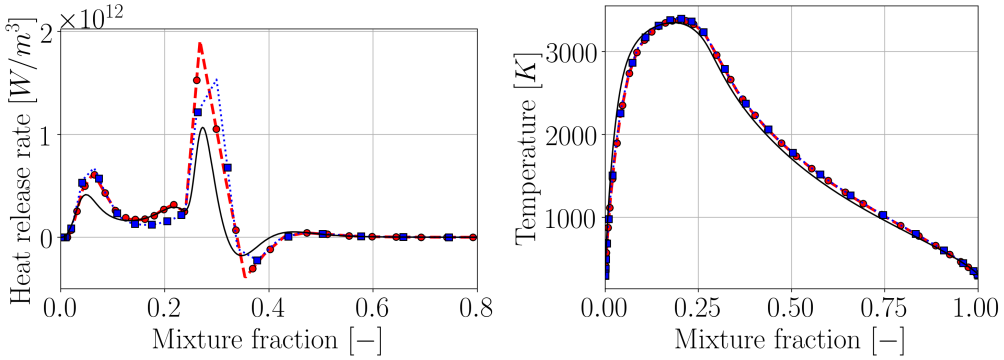

FIGURE 4. Heat release (left) and temperature (right) profiles in strained counterflow diffusion flame. Comparison between the classical (dashed-line), exponential (dotted-line) chemical integration methods and the CANTERA 1D flame (solid line). Coarse mesh.

istry is run with the CFL timestep, here about $\tau_{CFL} = 2.5ns$, while the simulation with the classic integration is run with the chemical timestep, defined in the simulation as:

$$\tau_{chem} = min\left(\frac{\rho}{\dot{\omega}_k}\right), \tag{3.8}$$

which gives in that case $\tau_{chem} = 1ns$. Note that this chemical timestep changes a lot during the computation (it oscillates around $1ns$), impacting the quality of the solutions; this phenomenon will be further explained in Section 4.3. The computation with exponential chemistry is therefore 2.5 times faster on this test case.
Because no strong deviation is observed in both the fine and the coarse meshes between the two integration methods, the exponential one is used in the following.

4. LOx/GCH$_4$ test bench

4.1. *Experimental setup*

The experimental configuration is here briefly introduced, but more details can be found in [10]. It consists of a single coaxial injector combustion chamber fed by gaseous methane and liquid oxygen. It is 290mm long, has a square cross section of 12x12mm and is equipped with convergent-divergent nozzle with a trapezoidal geometry. The chamber is designed for a 20-25bar pressure range. On the top on the combustion chamber, a 14.8mm thick window is mounted at the injector region. Therefore a gaseous nitrogen injection is used to cool down the window surface during firing tests. Otherwise the rest of the combustion chamber is capacitively cooled making use of the copper high thermal conductivity (19mm thick). The summary of the geometry can be found in Table 3 and the visual of the configuration is shown Fig. 5.

Several operating points have been already run and are detailed in [10]. For the present LES, the chosen operating point is sum up in Table 4.
The instrumentation allows to get temperature longitudinal profiles, thanks to 17 thermocouples with a spacing of 17mm all along the bottom wall of the combustion chamber. The static pressure is taken at 9 positions with a spacing of 34mm, stating 0.5mm downstream the faceplate.

Chamber length	[mm]	290
Chamber width	[mm]	12
Chamber heigth	[mm]	12
LOx diameter	[mm]	3
Lip thickness	[mm]	1
GCH4 inner diameter	[mm]	5
GCH4 outer diameter	[mm]	6

TABLE 3. Main geometrical parameters, without the nozzle

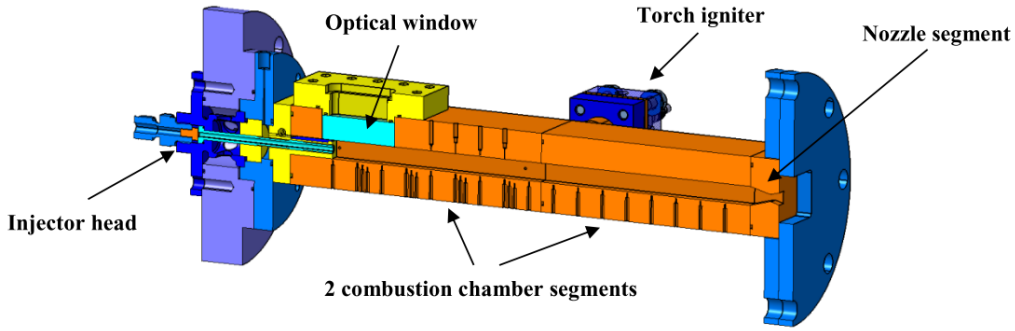

FIGURE 5. Combustion chamber with cryogenic injector head and optical access window [10]

Pressure	[bar]	20
LOx mass flow rate	[g/s]	46.51
GCH4 mass flow rate	[g/s]	15.5
GN2 mass flow rate	[g/s]	3.1
Mixture ratio	[-]	3.0
LOx temperature	[K]	96.8
GCH4 temperature	[K]	268.1
GN2 temperature	[K]	293

TABLE 4. Operating point for the LES

4.2. *Numerical setup*

4.2.1. *Geometry and mesh*

The full 3D combustion chamber is computed without the nozzle. Only a small part of the coaxial injector is modeled (2mm length). The injection and atomization of LOx are not resolved, but rather modeled as further explained in paragraph 4.2.2. In this model, the liquid jet formed by the LOx injection is replaced by a solid cone as shown Fig. 6 and 7.

The mesh about 64 million cells is fully tetrahedral. The post-lip and flame zone are particularly refined: characteristic mesh size at the lip is $\Delta_0 = 20\mu m$ and is progressively coarsened to $\Delta_c = 600\mu m$ at $x = 150mm$. At the walls, the boundary layer is also made of tetrahedra and the mesh results of y^+ values from 130 to 200 along the chamber. An overview is presented Fig. 6.

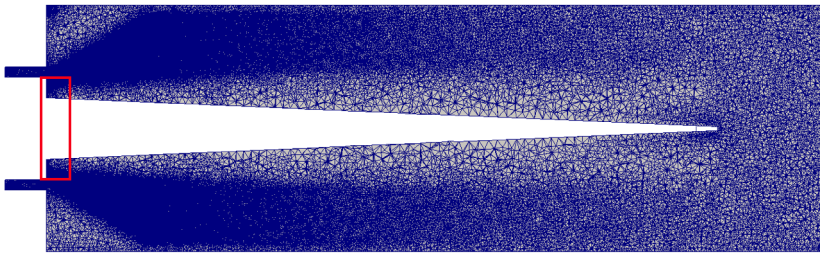

FIGURE 6. Mesh (Z-axis cut): zoom at the liquid oxygen cone (rest of the domain is about 6 times longer). The red box indicates where the scalar dissipation rate has been mesured to derive the ARC.

4.2.2. *Models*

The simulation is run with the LES solver AVBP, developed by CERFACS and IFPEN. It solves the compressible Navier-Stokes equations for unstructured meshes in an explicit way [27]. For convection, the second order in and space Lax-Wendroff scheme is used [28]. The turbulent closure is made thanks to the Sigma model [29]. The Soave-Redlich-Kwong equation of state if used [30] because of the cold oxygen injection. Constant turbulent Schmidt and Prandtl numbers (fixed at 0.7 for both) are used for the sub-grid diffusion and thermal terms. The power-law function is utilized for the molecular viscosity, and constant Schmidt and Prandtl numbers are used for species molecular diffusion and thermal conductivity. Local filtering on density and pressure is applied and takes the form of the LAD model [27].

Combustion chemistry is described with the ARC scheme derived Section 2, and integrated with the exponential time-integration method of Section 3. In the context of Thickened Flame Model [31], diffusion flames which are already artificially thickened by the mesh do not require further thickening. Subgrid-scale flame-turbulence interactions however remain, which in principle should be modeled. In the present case these effects are assumed small in comparison to the resolved turbulence thanks to the refined mesh and are omitted. It will be checked a posteriori that the flame is indeed a purely nonpremixed flame and that subgrid-scale turbulence is weak.

The LOx atomization is modelled following the work of Potier [32] and is briefly summarized here. The idea is to model the liquid cone of oxygen thanks to correlations, here the Woodward correlation [33] based on a predicted Weber number and liquid Reynolds number. The Woodward correlations gives the cone length, and from here, other parameters used in the model (see Fig. 7) are found: details can be found in [32]. These parameters are summarized in Table 5.

4.2.3. *Boundary conditions*

The boundary conditions are formulated with the NSCBC approach [34]. Inlets are set with the recent Non-Reflective Inlets (NRI) method [35] which allows to absorb acoustics while maintaining the target fluxes. As the nozzle is not computed, the outlet is set at 20 bar. At the the GCH_4 and GN_2 inlets, turbulent velocity profiles are imposed. The inlet walls use adiabatic no-slip conditions. The chamber walls are separated in two zones: one corresponding to the optical window, the other to the copper walls. Both

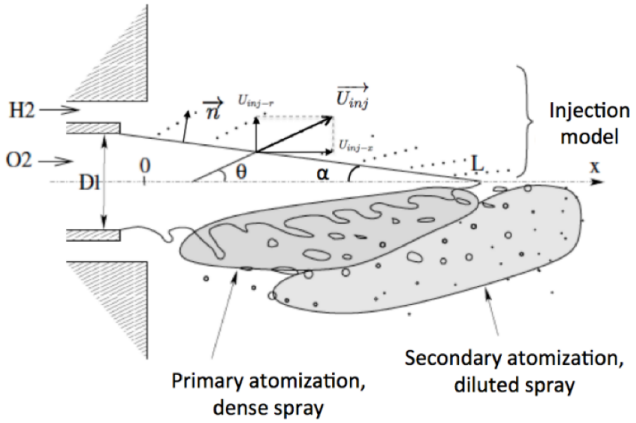

FIGURE 7. LOx atomization model overview (from [32])

Momentum flux ratio	[-]	27.11
Weber	[-]	49700
Droplets diameter (constant)	[μm]	30.10
Cone length (L)	[mm]	32.92
Injection angle (θ)	[deg]	33.87
Liquid fraction	[-]	0.064

TABLE 5. LOx particles injection parameters

make use of the coupled wall law derived by Cabrit [36], which takes into account the high temperature gradients expected between the burnt gases and the walls in a combustion chamber. The heat transfers through the wall thickness is taken into account by imposing a reference temperature (set at 293.15K here) and a thermal resistance for the window and the copper. The boundary conditions are sum up Fig. 8.

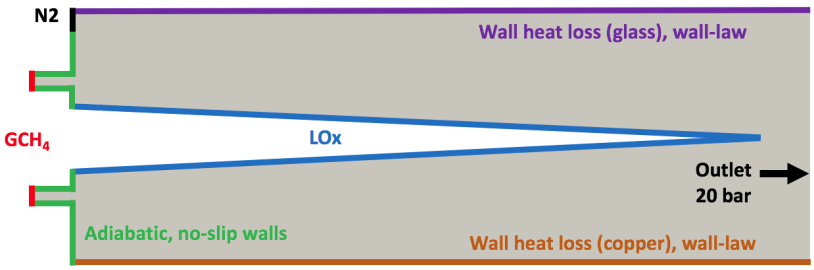

FIGURE 8. Boundary conditions

All inlets/outlets are considered as exits for the LOx droplets. Their interaction with walls are limited to rebound: no splash (separation of particles in several smaller particles) or liquid film are considered here, as they are not important phenomena in the studied case.

4.3. *Results*

Comparison between the classical integration of chemistry and the exponential one is first made on instantaneous fields taken at the same time. Both simulations were run different timestep. The classical integration of chemistry requires a chemical timestep $\tau_{chem} = 0.31ns$ here. The exponential integration is run with the CFL timestep about $\tau_{CFL} = 2.52ns$.
Therefore, a computational gain factor of about $\tau_{CFL}/\tau_{chem} = 8.1$ is obtained.

A look at the flame for both cases (Fig. 9 and 10) gives more insight about the effect of chemical integration:

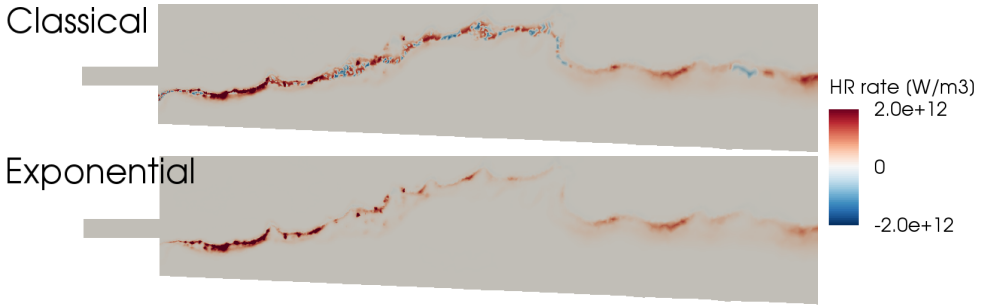

FIGURE 9. Heat release rate instantaneous field near the liquid cone. Top: classical integration. Bottom: exponential integration.

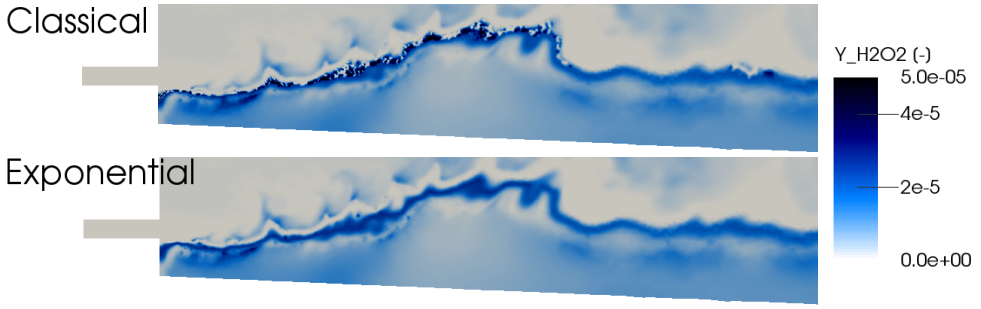

FIGURE 10. H_2O_2 mass fraction instantaneous field near the liquid cone. Top: classical integration. Bottom: exponential integration.

The heat release (Fig. 9) is much impacted by the time integration method: with classical chemistry, much noise is observed which is not related to mesh under-resolution but is the result of a too large timestep.
Indeed classical chemistry with chemical timestep leads to locally zero or even negative concentrations of the stiffest species such as H_2O_2 in Fig. 10.
These phenomena do not happen at all with the exponential integration. Indeed as mentioned in Section 3, the computed concentration always remain positive. Exponential integration must be however used with care as too high timesteps could miss some peaks (of mass fraction, source terms...) and accuracy could be lost locally. It was already verified in Section 3 that this did not happen in the laminar test case and the same kind of verification are now made for the 3D case.

Scatterplots of temperature and reactant mass fractions are built from an averaged solution in the close injector region and Fig. 11. They are compared to a CANTERA solution at $a_{mean} = 47500s^{-1}$, typical of measured values in this zone (the same as the red box in Fig. 6).

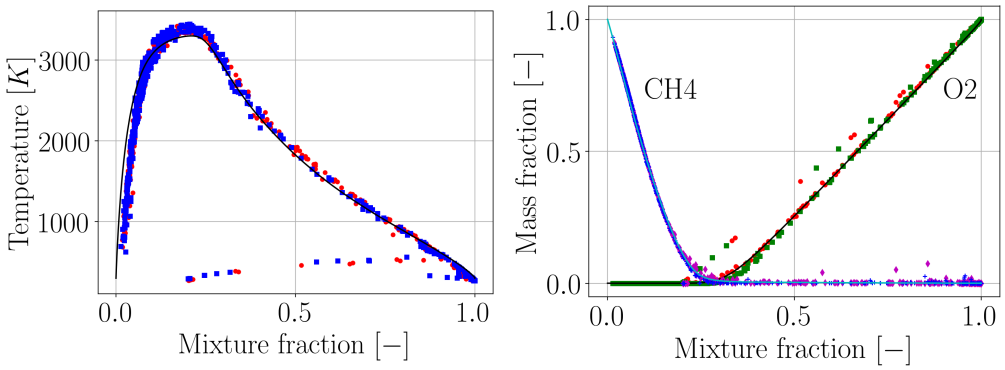

FIGURE 11. Scatterplots in the post-lip region. Left: temperature (solid line: CANTERA; circles: classical integration; squares: exponential integration). Right: reactants (solid line: CANTERA; circles: CH4, classical integration; squares: CH4, exponential integration; diamonds: O2, classical integration; crosses: O2, exponential integration)

In the 3D simulation again both integration methods show very similar results. They match well with the CANTERA solution, with slight dispersion due to turbulence. One can remark that some points of the scatterplots are not on the expected profiles: this is the trace of some liquid oxygen droplets which are able to cross the flame and evaporate further, as shown Fig. 13. Therefore some unburnt mixing is found. Except for these few isolated droplets the profiles show a pure diffusion flame.

The power generated by the flame (cumulative of heat release) is shown Fig. 12.

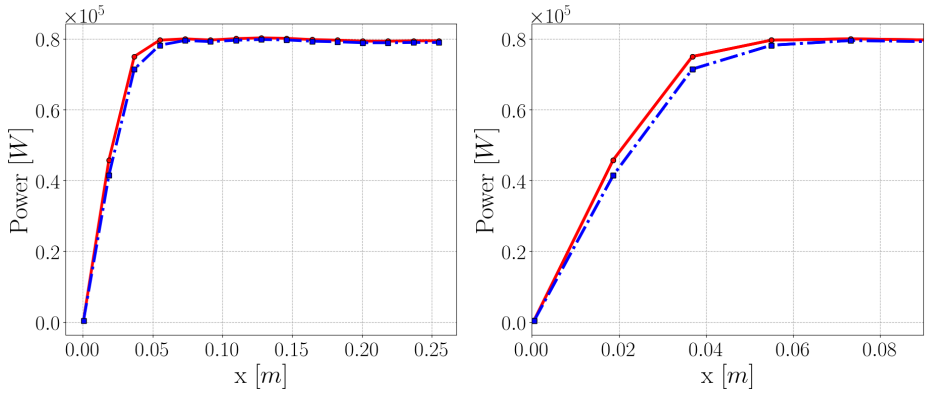

FIGURE 12. Left: cumulative heat release generated by the flame along the combustion chamber (average solution on $3\mu s$). Solid line: classic integration. Dashed-dotted line: exponential integration. Right: same but zoom on the flame region.

The two chemical models have a very fair agreement: the cumulative heat release exhibit only 0.6% gap at the end of the domain. The largest deviation is found between $x = 0.03m$ and $x = 0.05m$, right after the liquid oxygen cone: also where the mesh starts to be coarser. From this figure the flame length is evaluated around 7 cm.

Finally the structure of the two-phase flow flame is shown in Fig. 13.

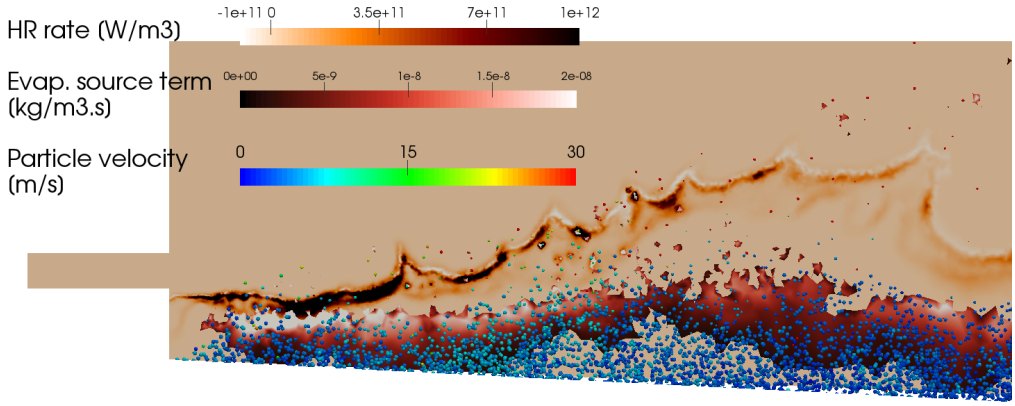

FIGURE 13. Two-phase flow interaction with the flame: heat release rate in background, with the evaporation source term between the liquid cone and the flame. The particles are represented by the dots colored with their velocity.

Fig. 13 shows that the LOx evaporation mostly happens before interacting with the flame zone, located by the heat release. As already seen in the scatterplots some droplets cross the flame: interestingly those have the highest velocity. Indeed as all droplets have the same size at injection, only their velocity can give them different behaviors. To be able to cross the flame, droplets must have a short convection time compared to evaporation time. These droplets then evaporate in the fuel side as observed in the top-right corner, where spots of evaporation are present. This is also the case more downstream in the chamber, not shown here. Nevertheless as the test bench operates overall in fuel-rich conditions, the oxygen is finally evaporated and burnt further and none is found at the outlet.

5. Conclusion

The single element LOx/GCH$_4$ TUM's combustion chamber has been computed with Large Eddy Simulation. With the will to perform a methane oxycombustion LES with a specific kinetic modelling for it, an Analytical Reduced Chemistry has been derived for the test case. The objective was not to have a general kinetic model for methane oxycombustion but rather to target an operating point in order to reduce as much as possible its complexity - so its cost. It is now feasible thanks to the friendly-user derivation code ARCANE, which will be used in the future to derived other ARCs, for other configurations.
Such level of chemical modelling leads to a high stiffness, and therefore too small computational timestep for an LES simulation: to overcome this issue a new integration method for chemical source terms has been proposed. Relying on the fact that it en-

sures positive concentrations, it reinforces the code stability and allows to use a larger timestep, even with ARC chemistry. Deeper analysis is foreseen to evaluate the wider use of exponential chemistry.
The new integration method allows to use the CFL timestep for the LES computation with an ARC in the test bench simulation. The simulation of the whole test bench is still ongoing. First results are promising, especially in terms of computational cost which remains a limiting aspect of using LES.

Acknowledgments

This work has been funded by CNES (Centre National d'Etudes Spatiales) and ArianeGroup in the context of S. Blanchard PhD work. Financial support has been provided by the German Research Foundation (Deutsche Forschungsgemeinschaft – DFG) in the framework of the Sonderforschungsbereich Transregio 40. The authors acknowledge CINES (Centre Informatique National de l'Enseignement Supérieur) and IDRIS (Institut du Développement et des Ressources en Informatique Scientifique) of GENCI (Grand Equipement National de Calcul Intensif) for giving access to HPC resources under the allocation A0052B10157. Finally special thanks are adressed to Luc Potier, Quentin Cazères, Théo Ogier and Jonathan Wirtz for their advices setting up the numerical simulations, as well as Oskar Haidn, Nikolaos Perakis and Christoph B. von Sethe for providing the test case and fruitful discussions.

References

[1] JONES, H.W. (2018). The Recent Large Reduction in Space Launch Cost. *4th International Conference on Environmental Systems*, (July), 1–10.

[2] NEILL, T., JUDD, D., VEITH, E. AND ROUSAR, D. (2009). Practical uses of liquid methane in rocket engine applications. *Acta Astronautica*, **65**(5-6), 696–705. ISSN 00945765. DOI 10.1016/j.actaastro.2009.01.052.

[3] PERIGO, D. ET AL. *LOX / Methane Gap Assessment Report*. Tech. rep.

[4] PRECLIK, D., HAGEMANN, H., O., K., MAEDING, C., HAESELER, D., HAIDN, O., WOSCHNAK, A. AND DEROSA, M. (2005). LOX/hydrocarbon preparatory thrust chamber technology activities in Germany. *41st AIAA/ASME/SAE/ASEE Joint Propulsion Conference and Exhibit*, (July), 1–15.

[5] KLEM, M.D. *LOX/Methane In-Space Propulsion Systems Technology Status and Gaps*. Tech. rep.

[6] SUTTON, P.G. (2003). *History of Liquid Propellant Rocket Engines*.

[7] PREUSS, A., PRECLIK, D., MADING, C., GORGEN, J., SOLLER, S., HAIDN, O., OSCHWALD, M., CLAUSS, W., ARNOLD, R. AND SENDER, J. (2008). LOX/Methane Technology Efforts for Future Liquid Rocket Engines. (May).

[8] SILVESTRI, S., CELANO, M.P., SCHLIEBEN, G., KIRCHBERGER, C. AND HAIDN, O.J. (2008). Characterization of a GOX-GCH4 Single Element Combustion Chamber. *TUM*, **1**(October), 352–362.

[9] SILVESTRI, S., CELANO, M.P., SCHLIEBEN, G. AND HAIDN, O.J. Characterization of a Multi-Injector GOX/CH4 Combustion Chamber. *52nd AIAA/SAE/ASEE Joint Propulsion Conference*, 1–14. DOI 10.2514/6.2016-4992.

[10] VON SETHE, C.B., SOLLER, S. AND HAIDN, O.J. (2019). Experimental investigation of a single element LOX / GCH4 heat-sink combustion chamber. *Eucass 2019*, (July).

[11] LACAZE, G., CUENOT, B., POINSOT, T. AND OSCHWALD, M. Large eddy simulation of laser ignition and compressible reacting flow in a rocket-like configuration. *Combustion and Flame*, (6), 1166–1180. ISSN 00102180. DOI 10.1016/j.combustflame.2009.01.004.

[12] SCHMITT, T., MÉRY, Y., BOILEAU, M. AND CANDEL, S. (2011). Large-Eddy Simulation of oxygen/methane flames under transcritical conditions. *Proceedings of the Combustion Institute*, **33**(1), 1383–1390. ISSN 15407489. DOI 10.1016/j.proci.2010.07.036.

[13] MAESTRO, D., CUENOT, B. AND SELLE, L. (2019). Large Eddy Simulation of Combustion and Heat Transfer in a Single Element GCH4/GOx Rocket Combustor. *Flow, Turbulence and Combustion*. ISSN 15731987. DOI 10.1007/s10494-019-00036-w.

[14] LI, D., ZHANG, Q., MA, Q. AND SHEN, S. Comparison of explosion characteristics between hydrogen/air and methane/air at the stoichiometric concentrations. *International Journal of Hydrogen Energy*, (28), 8761–8768. ISSN 03603199. DOI 10.1016/j.ijhydene.2015.05.038.

[15] GRIFFITHS, J.F. (1995). Reduced kinetic models and their application to practical combustion systems. *Progress in Energy and Combustion Science*, **21**(1), 25–107. ISSN 03601285. DOI 10.1016/0360-1285(94)00022-V.

[16] LU, T. AND LAW, C. (2006). Systematic approach to obtain analytic solutions of quasi steady state species in reduced mechanisms. *Journal of Physical Chemistry A*, **110**(49), 13202–13208. ISSN 10895639. DOI 10.1021/jp064482y.

[17] FELDEN, A., PEPIOT, P., ESCLAPEZ, L., RIBER, E. AND CUENOT, B. Including analytically reduced chemistry (ARC) in CFD applications. *Acta Astronautica*, 444–459. ISSN 00945765. DOI 10.1016/j.actaastro.2019.03.035.

[18] FELDEN, A., JARAVEL, T., RIBER, E., CUENOT, B. AND PEPIOT, P. (2016). Predicting pollutant emissions in complex burners using analytically reduced chemistry. In: *MUSAF III*. ONERA, Toulouse, France.

[19] FELDEN, A. (2013). *Development of Analytically Reduced Chemistries (ARC) and applications in Large Eddy Simulations (LES) of turbulent combustion*. Ph.D. thesis.

[20] KEE, R.J., PETZOLD, L.R., SMOOKE, M.D. AND GRCAR, J.F. *Implicit Methods in Combustion and Chemical Kinetics Modeling*. ACADEMIC PRESS, INC. ISBN 0121234207. DOI 10.1016/b978-0-12-123420-1.50010-0.

[21] SMITH, G.P., GOLDEN, D.M., FRENKLACH, M., MORIARTY, N.W., BORIS EITENEER, M.G., BOWMAN, C.T., HANSON, R.K., SONG, S., GARDINER, W.C., LISSIANSKI, V.V. AND QIN, Z. URL `http://combustion.berkeley.edu/gri-mech/`.

[22] PETERSEN, E.L., DAVIDSON, D.F. AND HANSON, R.K. (1999). Kinetics modeling of shock-induced ignition in low-dilution CH4/O2 mixtures at high pressures and intermediate temperatures. *Combustion and Flame*, **117**(1-2), 272–290. ISSN 00102180. DOI 10.1016/S0010-2180(98)00111-4.

[23] SLAVINSKAYA, N.A., ABBASI, M., WEINSCHENK, M. AND HAIDN, O.J. Methane Skeletal Mechanism for Space Propulsion Applications.

[24] PEPIOT, P. AND CAZERES, Q. ARCANE website. URL `https://chemistry.cerfacs.fr/en/arcane/`.

[25] BILGER, R.W. (1989). The structure of turbulent nonpremixed flames. *Symposium (International) on Combustion*, **22**(1), 475–488. ISSN 00820784. DOI 10.1016/S0082-0784(89)80054-2.

[26] SHUM-KIVAN, F. (2017). *Simulation des Grandes Echelles de flammes de spray et modélisation de la combustion non-prémélangée*. Ph.D. thesis.

[27] AVBP website. URL `http://www.cerfacs.fr/avbp7x/`.

[28] LAX, P., .W.B. (1960). Systems of conservation laws. Communications on Pure and Applied Mathematics. *Combustion and Flame*, (13(2)), 217âĂŞ237. DOI 10.1002/cpa.3160130205.

[29] NICOUD, F., TODA, H., CABRIT, O. ET AL. (2011). Using singular values to build a subgrid-scale model for large eddy simulations. *Physics of Fluids*.

[30] SOAVE, G. (1972). Equilibrium constant from a modified Redlich-Kwong equation of state. *Chemical Engineering science*, **27**(6), 1197–1203.

[31] COLIN, O., DUCROS, F., VEYNANTE, D. AND POINSOT, T. (2000). A thickened flame model for large eddy simulations of turbulent premixed combustion. *Physics of Fluids*, **12**(7), 1843–1863. ISSN 10706631. DOI 10.1063/1.870436.

[32] POTIER, L. (2018). *Large Eddy Simulation of the combustion and heat transfer in sub-critical rocket engines*. Ph.D. thesis.

[33] BRAY, K.N.C. AND PETERS, N. (1994). *Laminar flamelets in turbulent flame*. Academic Press, London, 63–113.

[34] POINSOT, T. AND LELE, S. Boundary conditions for direct simulations of compressible viscous flows. *Journal of Computational Physics*, (2), 352. ISSN 00219991. DOI 10.1016/0021-9991(92)90227-P.

[35] DAVILLER, G., OZTARLIK, G. AND POINSOT, T. A generalized non-reflecting inlet boundary condition for steady and forced compressible flows with injection of vortical and acoustic waves. *Computers and Fluids*, 503–513. ISSN 00457930. DOI 10.1016/j.compfluid.2019.06.027.

[36] CABRIT, O. AND NICOUD, F. (2009). Direct simulations for wall modeling of multicomponent reacting compressible turbulent flows. *Physics of Fluids*, **21**(5), 0–29. ISSN 10706631. DOI 10.1063/1.3123528.